Laser-assisted and field-free ionization cross sections of the He(2 ¹S,2 ³S)+He(1 ¹S) collision system

P. Pradel, P. Monchicourt, D. Dubreuil, and J. J. Laucagne

Service de Physique des Atomes et des Surfaces, Centre d'Etudes Nucléaires de Saclay, 91191 Gif-Sur-Yvette Cedex, France

(Received 1 May 1986)

A study of the laser-assisted and field-free ionization cross sections of the He*(2 ¹S,2 ³S)+He(1 ¹S) collision system is presented as a function of the kinetic energy of the collision. The work of Evans *et al.* [Phys. Rev. A **4**, 2235 (1971)] and Cohen [Phys. Rev. A **13**, 86 (1976)] on the He₂* molecular system is used to calculate the value σ_d of the field-free ionization cross section and then to normalize our experimental results. Knowing σ_d, we deduce the assisted-ionization cross section σ_a. These data show that within our energy range, the main process below $E_{c.m.} = 50$ eV is laser-assisted ionization, whereas above this kinetic energy, it is a two-step reaction: collisional excitation followed by the photoionization of the level reached.

I. INTRODUCTION

The effect of a strong electromagnetic field on the dynamics of an atomic collision, first emphasized and studied by Gudzenko and Yakovlenko,[1] has stimulated an impressive amount of theoretical[2-14] and experimental work.[14-28] The principal characteristic of these processes termed "laser-assisted collisions" is that the photon absorption occurs only in the course of the collision. New inelastic events become possible, since a quantum of energy is introduced by the photon in addition to the kinetic energy of the colliding partners. Among these processes, laser-assisted ionization is conceptually one of the simplest, but is experimentally one of the most difficult to study. On the one hand, it seems attractive to investigate systems having their final state embedded in a continuum, since they have the obvious advantage that the product charged particles are easy to detect. On the other hand, however, the nonresonant nature of the radiative transition is characterized by the lack of large cross sections and the absence of collision-broadening spectroscopy[29,30] both essential for the experimental study of laser-assisted collisions involving a bound-bound transition.[15-21] The smallness of assisted ion signals has led experimentalists to use thermal beams[22-24] or vapors,[25,26] that is, media with high atomic reactant densities. As a result, it is very difficult to isolate the assisted ionization from other competing channels, involving for instance an energy-pooling collision[31] or a dimer photoionization.[32-34] A completely different approach is used in the present work, where the simplest possible colliding system is used in order to single out the assisted process from possible competing mechanisms. This is achieved with a very-low-density beam with kinetic energy of a few tens of eV's impinging on an atomic target under single-collision conditions in the presence of a laser beam. In this experiment, monitoring the relative kinetic energy of the colliding system is a powerful tool for distinguishing the assisted signal from other signals by its characteristic dependence on kinetic energy.

We have chosen the well-known helium system He*(2 ¹S,2 ³S)+He(1 ¹S) which has been extensively studied, both theoretically[35-39] and experimentally[40-43] under field-free conditions. We report here measurements of the He⁺ signal resulting from the following laser-assisted process:

$$\text{He}^*(2\,^1S, 2\,^3S) + \text{He}(1\,^1S) + \hbar\omega$$

$$\rightarrow \text{He}^+(1\,^2S) + \text{He}(1\,^1S) + e^- , \quad (1)$$
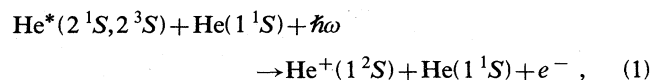
where He*(2 ¹S,2 ³S) are the two metastable levels of the helium atom lying 4.0 and 4.8 eV, respectively, below the He⁺(1 ²S)+e⁻ continuum limit. The potential curves of the collision system of Refs. 36 and 39 are plotted in Fig. 1. Photon absorption occurs by a bound-free transition between the two initial states 2 ¹Σ_g and 2 ³Σ_g and the final continuum state above the first ionization limit. The photon energy $\hbar\omega = 3.49$ eV is below the photoionization threshold for He*(2 ¹S,2 ³S) and is not resonant with any atomic transition of the separated partners. The lowest energy gap is of the order of 480 cm⁻¹ and corresponds to the difference between the field-dressed 2 ¹S level and the 5 ¹P level (see Fig. 1). Ionization occurs by the simultaneous action of the field and collisional perturbations, that is, when the initial and final potential curves become close enough to allow photon absorption and electron ejection. This is shown in Fig. 1 by the 2 ¹Σ_g +ℏω and 2 ³Σ_g +ℏω field-dressed curves. Ionization becomes possible when these two curves enter the continuum, i.e., for internuclear distances $R \leq R_0$, where $R_0 = 2.25$ Å for the 2 ¹Σ_g curve, and $R_0 = 1.95$ Å for the 2 ³Σ_g. This process can be viewed as a photoionization of the transient molecule whose "lifetime" is less than $2R_0/v$ (which is the limit corresponding to a frontal collision), where v is the relative velocity of the two atoms. Only fast He⁺ ions from He* metastable and having roughly the same kinetic energy are detected. Hence, a selective study of the assisted collision (1) involving a one-electron transition is carried out. This process, where the He(1 ¹S) atom acts only as a perturber, differs markedly from Penning assisted ionization which involves an electron transition in each atom[44]; it should be noted that the validity of the quantal scheme
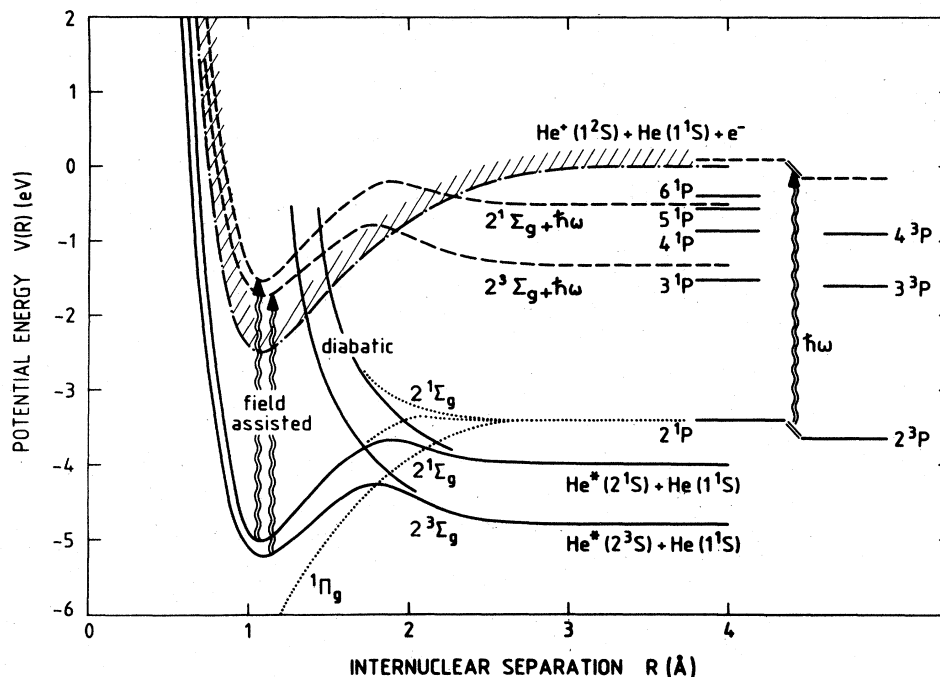
FIG. 1. Relevant adiabatic potential curves for He_2^* and He_2^+ obtained from Ref. 39. The diabatic curves correlated with the two entrance channels have been taken from Ref. 36. Dashed lines represent the field-dressed potential curves.

in terms of photoionization and field-dressed curves depends on the magnitude and time scale of both collision and field perturbations. Therefore the lifetime of the molecule, that is the interval of time available for photon absorption, has to be much larger than the laser field period ω; also, the laser light power density has to be moderately high in order to avoid multiphoton absorption processes. Such validity will be discussed in Sec. IV. In Sec. II the experimental arrangement is presented. The experimental procedure and the results are given in Sec. III. This section includes (i) the identification and discrimination of the assisted ion signal from the ions produced by a well-known field-free diabatic process (ii) the determination of the absolute value of field-free and assisted signals by utilizing a theoretical value for the field-free diabatic cross section for calibration, and (iii) studies of the laser-assisted cross section as a function of laser intensity and relative kinetic energy. Finally, our results are discussed in Sec. IV and compared with theoretical estimates.

II. APPARATUS

A schematic view of the apparatus is given in Fig. 2. Details of the apparatus used to measure laser-assisted ionization and field-free ionization cross sections have been described elswewhere.[27]

A. Ion source

A He^+ ion beam is extracted from a water-cooled Colutron source consisting of a hot-cathode positive-ion glow discharge maintained by electrons having a max-

imum energy of 100 eV. The ions are extracted through a 0.5-mm-diam aperture in a molybdenum anode. They are accelerated by a negatively biased electrode, which is also the first element of a cylindrical lens (einzel lens). After this first focusing, the He^+ beam is decelerated and focused again by a Menzinger retardation system, from 500-eV initial energy to the desired ajustable working energy: this procedure ensures a higher source efficiency. The working energies of the ions, given in the text, result from the accelerating voltage of the ion-source anode with respect to the ground potential.

In order to eliminate the fast neutral He atoms produced by charge-exchange in the residual gas of the region near the ion source (see Fig. 2), the first section of the apparatus, including the ion source, the focalization lens, and the Menzinger decelerator is slightly rotated in the horizontal plane. These fast neutral atoms are mainly produced by the resonant reaction

$$He^+ + He \rightarrow He + He^+ \qquad (2)$$

which is efficient in the region between the anode and decelerator, where the background pressure is of the order of 10^{-5} torr. The He^+ beam is deflected and adjusted on the geometrical axis of the second section by a $7°$ magnetic selector.

B. Neutralization cell

Atoms in the $2\,^1S$ and $2\,^3S$ excited states of He are formed by near-resonant charge transfer between He^+ ions and an alkali-metal vapor contained in an oven filled
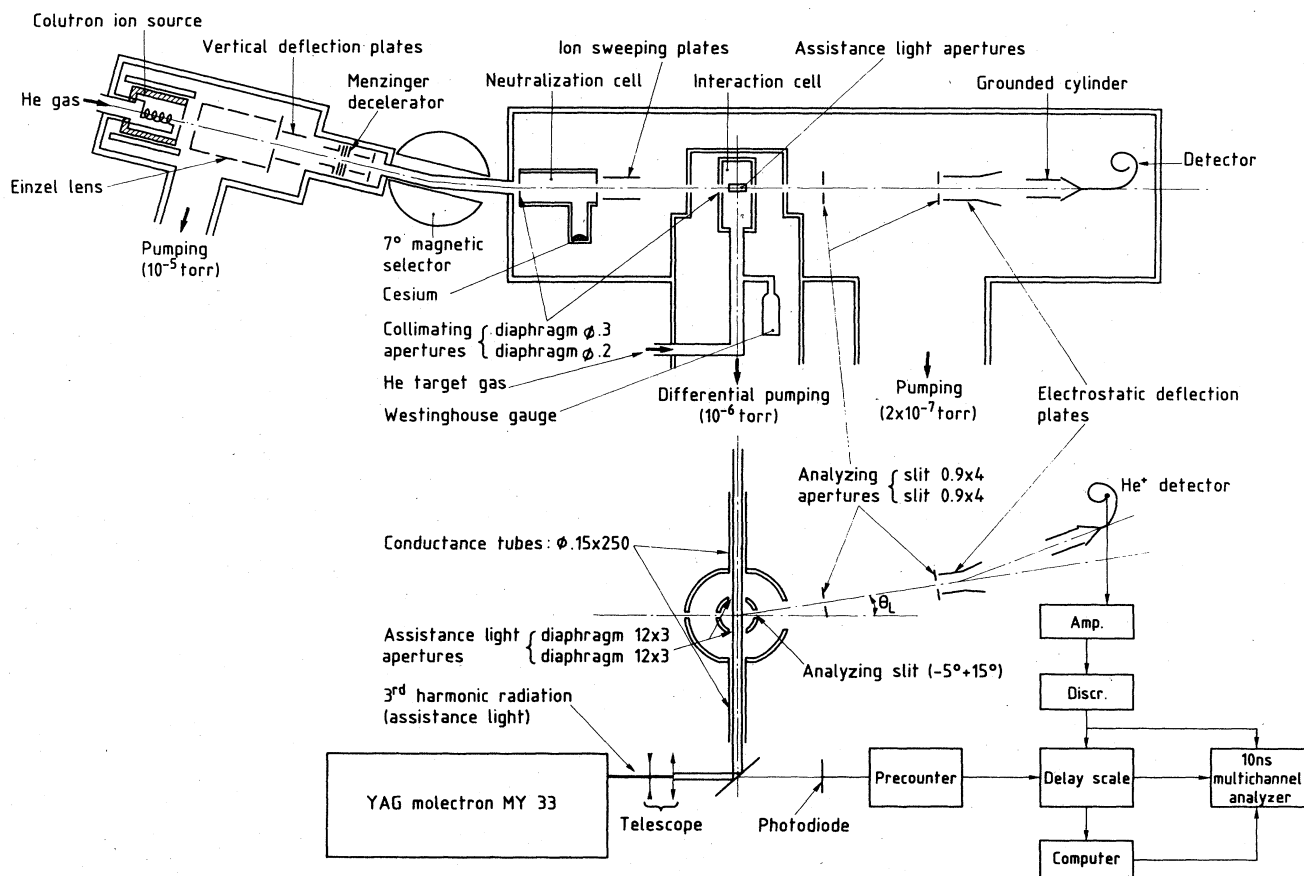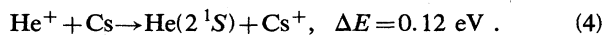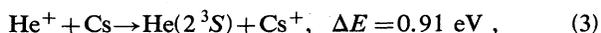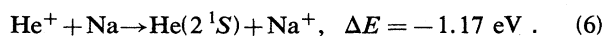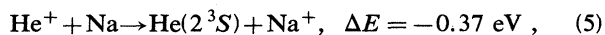
FIG. 2. Schematic diagram of the apparatus. The drawing is not to scale. Dimensions are in millimeters. Measurements have been performed for $\theta_L = 0°$.

with either cesium[42] or sodium[45] at pressures ranging from 4×10^{-6} to 2×10^{-4} torr (depending on the working energy). For the cesium target, neutralization occurs through the quasiresonant reactions

$$\text{He}^+ + \text{Cs} \rightarrow \text{He}(2\,^3S) + \text{Cs}^+, \quad \Delta E = 0.91 \text{ eV} , \quad (3)$$

$$\text{He}^+ + \text{Cs} \rightarrow \text{He}(2\,^1S) + \text{Cs}^+, \quad \Delta E = 0.12 \text{ eV} . \quad (4)$$

In the Na case we have

$$\text{He}^+ + \text{Na} \rightarrow \text{He}(2\,^3S) + \text{Na}^+, \quad \Delta E = -0.37 \text{ eV} , \quad (5)$$

$$\text{He}^+ + \text{Na} \rightarrow \text{He}(2\,^1S) + \text{Na}^+, \quad \Delta E = -1.17 \text{ eV} . \quad (6)$$

When leaving the neutralization cell the neutral beam consists of helium atoms in (i) the metastable triplet $2\,^3S$ state, (ii) the metastable singlet $2\,^1S$ state, and (iii) the $1\,^1S$ ground state. The relative abundances of the metastable components of the two alkali-metal vapor targets is known from the data obtained by Reynaud et al.[45] As far as the He($1\,^1S$) neutral beam abundance is concerned, this state arises from radiative deexcitation of the He($2\,^1P$) state which is not greatly excited; an upper limit of 10% can be estimated with reasonable confidence.[45] In the following considerations this state is not taken into account.

Any remaining ions are deflected from the beam by a weak transverse electric field applied between two plates immediately after traversing the oven; the remaining metastable beam passes into the interaction cell.

C. Interaction cell and beam measurements

The entrance aperture of this chamber is a diaphragm 2 mm in diameter, whereas the exit aperture permits measurements of scattered particles at angles between $-5°$ and $+15°$ with respect to the beam axis; the collision cell is 12 mm long. An Ionivac IM 110D ionization gauge is used to monitor the helium target pressure during the experiments: it was experimentally verified that this pressure ensured single-collision conditions, i.e., a linear dependence of the emerging metastable beam intensity on the pressure. A differential pumping system maintains a background pressure of 1×10^{-6} torr in the unit.

A stainless-steel Faraday cup with a secondary electron suppressor (not shown on Fig. 2) can be positioned after the gas cell on the beam axis: this enables the He$^+$ beam from the source to be both aligned and measured; the metastable He* beam is also detected from this cup by Auger deexcitation, the cylindrical suppressor bias being inverted to attract secondary electrons. The signal measured in these conditions is

$$I'^* = I^* \gamma^* , \qquad\qquad (7)$$

where I^* is the equivalent metastable current reaching the Faraday cup, γ^* is the secondary-electron ejection coefficient of the He* atom, and I'^* is the equivalent experimentally measured metastable current. Typically a $+35$ V extraction potential difference between the target and the suppressor cylinder is used; the positive current from the target is measured by a Keithley 610 C electrometer using an input resistance of 10^{14} Ω.

D. Assistance lasers

Inside the interaction cell the He* beam is crossed with an orthogonal laser light beam of rectangular cross section (Fig. 2). The assistance radiation is provided either by the third harmonic of a commercial (Molectron MY 33) Nd-doped yttrium aluminum garnet (YAG) laser ($\lambda = 355$ nm) or by light from a Lambda Physik excimer laser type EMG 102 using a XeF active medium ($\lambda = 351$ nm). The YAG laser routinely delivers 20-mJ light pulses with a $\tau = 20$ nsec duration time and a 10-Hz repetition rate, whereas the excimer laser delivers a maximum output energy of 60 mJ with $\tau = 14$ nsec and a 70 Hz repetition rate. In order to illuminate the whole of the collision volume, a telescope is used to transform the divergent laser beam into a parallel beam with a cross section $\sim 12 \times 2$ mm^2 where the average power density is ~ 5 MW cm^{-2} (Fig. 2).

E. Analyzing assembly

The scattered fast ions produced in the interaction chamber can be angularly analyzed by an assembly consisting essentially of two analyzing slits, an electrostatic deflection plate system, and a detector; the whole unit can be rotated about the vertical axis of the interaction cell (Fig. 2). The He$^+$ ions produced in the interaction cell and scattered in the θ_L direction defined by two rectangular slits (0.9×4 mm^2) 100 mm apart are discriminated from the residual scattered He* at the same angle by an appropriate transverse electric field between two half-cylinder-shaped plates: the He$^+$ ions impinge on the detector which is an RTC channeltron model X 419 BL located in a grounded box. As the experimental axis lies along an Earth meridian, the vertical component of the Earth's magnetic field can be compensated for by passing a suitable current through a rectangular coil surrounding the entire apparatus.

III. EXPERIMENTAL METHOD

The assisted collisional ionization studied in this paper is defined by reaction (1), hence, the corresponding assisted-ionization cross section σ_a, measured in this work, does not distinguish between the two excited states. However, above a few tens of eV (approximately $E_L = 40$ eV in the laboratory), the metastable kinetic energy becomes sufficient for the field-free collisional ionization of the system studied to occur via a known diabatic non-resonant channel[42] (see Fig. 1)

$$\text{He*}(2\,^1S, 2\,^3S) + \text{He}(1\,^1S)$$

$$\rightarrow \text{He}^+(1\,^2S) + \text{He}(1\,^1S) + e^- . \qquad (8)$$
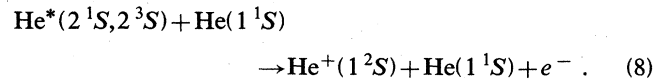
The corresponding cross section for the diabatic reaction is σ_d; the remark made for σ_a also applies in this case. The ions produced during the short laser pulse via the assisted process (1) are superimposed on the ion diabatic constant signal from reaction (8): these latter ions appear as a background added to the pulsed signal from the assisted reaction (1). Figure 2 shows the data acquisition system enabling the assisted ion signal to be distinguished from the diabatic background. A small part of the laser light is directed onto a photodiode delivering a pulse which simultaneously activates a precounter and a delayed scaler having a delay time of the same order as the ion time of flight between the interaction cell and the detector. The output pulse counts from the channeltron are amplified, discriminated from internal noise, and simultaneously fed into a fast multichannel analyzer and the delayed scaler, the latter serving as an ion monitor. The analyzer is activated about 1 μsec before the arrival of the assisted ions and is inhibited 2.5 μsec later, in order to record over a relatively long period of time the known continuous diabatic signal, the average of which is used to calibrate the assisted ion peak.[42] The scan of the analyzer is comprised of 50 channels, each 50 nsec in duration. In this paper we only report measurement for a zero scattering angle where the ion signals present the best statistics.

Figure 3 shows a typical histogram of the data. Histograms such as those of Fig. 3 are recorded with the same number of laser shots ($\alpha = 6 \times 10^5$) and normalized to the same irradiation conditions (~ 5 MW cm^{-2}). The averaged value $\bar{S}_d$ of the ion diabatic signal and the peak value S_a of the assisted ion signal are shown in this figure. The peak is localized in the window calculated on the following considerations: (i) the time of flight for as-
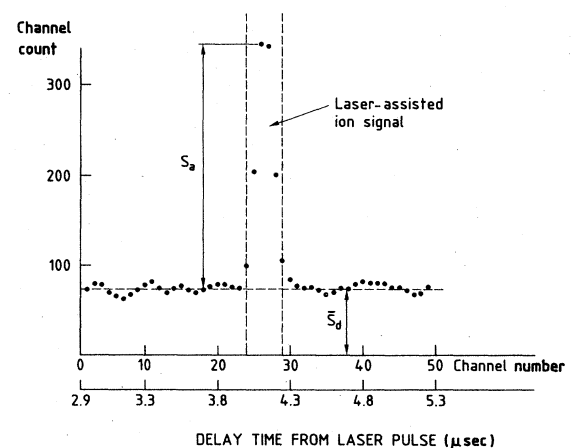

FIG. 3. Typical histogram of diabatic and assisted ion signals for $E_{c.m.} = 50$ eV and $W_p = 34$ mJ. The analyzer scans 50 channels each of which has a 50-nsec duration. The assisted signal window is surrounded by the pure field-free diabatic signal. $\bar{S}_d$ represents the averaged value of this signal. S_a is the maximum laser-assisted ion signal. The vertical dash-dotted lines represent the expected assisted-signal window (see Sec. III).

sisted ions produced in the middle of the interaction cell to reach the detector is β; this time is determined from the photodiode pulse and corresponds to the middle of the window. (ii) calculations of the width of this window which must include the He* atom crossing time t inside the cell, the laser pulse duration τ, and the beam energy spread effect Δt on the time of flight between the interaction cell and the detector. For example, for $E_{c.m.}=50$ eV, $v=6.92\times10^4$ m sec^{-1}, $\beta=4.1$ μsec, $t=173$ nsec, $\tau\sim20$ nsec, and full width at half maximum (FWHM) $\Delta t\sim\pm20$ nsec, the window width is 230 nsec (five channels); we measured $\bar{S}_d$ and S_a for various kinetic energies ranging from 25 to 150 eV in the center-of-mass system (50—300 eV in the laboratory system). Hence, for each of the energies considered, a histogram similar to the one shown in Fig. 3 was obtained; from these data σ_d and σ_a can be deduced as a function of energy through calculations of the signal integrals $\bar{S}_d$ and S_a based on the following considerations: Let n^* be the metastable atom density impinging on a He($1\,^1S$) target of density n_{He} (particles per cm^3); the ion density produced by reaction (8) is defined by the expression

$$\frac{dn_d^+}{dt}=\sigma_d n^* n_{He} v \ ,$$

where v is the relative velocity of the colliding partners. The interaction volume is $V=Sl$ [S is the cross-sectional area of the metastable beam and l is the interaction length (1.2 cm)]; if the metastable flux is defined as $F^*=n^*Sv$ (atoms sec^{-1}), the number of ions produced inside V during the interaction time l/v is

$$Vn_d^+=\sigma_d F^* n_{He}\frac{l^2}{v} \ .$$

For α analyzer scans (α is also the number of laser shots) we measure

$$D=k(E)Vn_d^+\alpha \ .$$

D is the integral of $\bar{S}_d$ over the interaction time l/v. $k(E)$ is the efficiency of the analyzing assembly which depends on the kinetic energy of the collision, so

$$D=k(E)\sigma_d F^* n_{He}\frac{l^2}{v}\alpha \ . \tag{9}$$

In contrast, the ion density produced by reaction (1) is given by

$$\frac{dn_a^+}{dt}=\sigma_a n^* n_{He} v \ .$$

The number of assisted ions produced in the interaction volume $\mathscr{V}=S(l+\tau v)$ illuminated by the assistance radiation during the laser pulse duration time τ (FWHM) is

$$\mathscr{V}n_a^+=\sigma_a F^* n_{He}\tau(1+\tau v) \ .$$

For α laser shots we measure

$$A=k(E)\mathscr{V}n_a^+\alpha \ .$$

A is the integral of the assisted ion signal S_a shown in Fig. 3; the efficiency of the analyzing assembly $k(E)$ is assumed to be the as in Eq. (9). Within $\pm10\%$ ($\mathscr{V}=Sl$), A is given by the following expression:

$$A=k(E)\sigma_a F^* n_{He}\tau l\alpha \ . \tag{10}$$

The common parameters are identical to those of Eq. (9).

The contrast C can be defined as follows:

$$C=\frac{A}{D}=\frac{\sigma_a v\tau}{\sigma_d l} \ . \tag{11}$$

C can hence be obtained from the recorded histograms, so

$$\sigma_a=\sigma_d C\frac{l}{\tau v} \ . \tag{12}$$

A. Measurement of the diabatic ionization cross section σ_d

From the histograms recorded for the different working energies, we obtain $\bar{S}_d=f(E)$ and the expression (9) can be written

$$\sigma_d\propto\frac{Dv}{k(E)F^*} \quad \text{or} \quad \sigma_d\propto\frac{\bar{S}_d}{k(E)F^*} \ , \tag{13}$$

n_{He}, l, α, and the analyzer channel duration time remaining constant in all the experiments.

1. Determination of I^*

Experimentally, we directly measure I'^* [Eq. (7)]. In order to determine I^* (directly related to F^* by the expression $F^*=I^*/e$), the secondary-electron ejection coefficient for the metastable atoms γ^* must be determined, this coefficient being a function of the metastable beam energy. In our energy range, it is reasonable to consider γ^+ (the secondary emission coefficient for He$^+$) as being a good approximation for γ^*.[47] The values of γ^* used in this work have taken from Ref. 47 and are reported in Table I.

TABLE I. Secondary emission coefficient γ^* for He* atoms on a "dirty" stainless-steel surface at normal incidence vs kinetic energy (Ref. 47).

$E_{c.m.}$ (eV)	25	30	35	50	60	75	100	150
γ^*	0.14	0.15	0.16	0.20	0.21	0.23	0.28	0.38

2. Angular scattering correction for
$k(E)$

The effect of the small acceptance of the analyzing assembly leads to a dependence of the $k(E)$ coefficient of relations (9) and (10) on angular scattering; this, therefore, makes the coefficient energy dependent. In order to take transmission effects into account, it is necessary to perform an angular analysis on the He^+ scattered signal at the different working energies. Figure 4 shows a typical He^+ scattering curve as a function of the laboratory angle θ_L recorded for $E_{c.m.} = 50$ eV. In our experimental conditions, this curve is proportional to the ionization differential cross section $d\sigma/d\omega$ $(\omega = \theta)$.[48] Neglecting the small variation in the interaction volume, for small scattering angles $(\theta_L < 6°)$ (Ref. 48) we deduce that the scattered He^+ flux reaching the detector from a direction θ (defined by its two components, θ_L in the horizontal plane and 0 in the vertical plane) is proportional to

$$\int \frac{d\sigma}{d\omega}(\omega)T(\theta-\omega)d\omega \ . \tag{14}$$

This expression is also proportional to $\overline{S}_d$ if $\theta=0$. ω is a variable direction and $T(\theta)$ is the transfer function of the analyzing assembly. This function has been calculated and depends on the dimensions and positions of the apertures as well as on the laboratory scattering angle θ_L throughout the interaction volume. The integral

$$\mathscr{D} = \int \frac{d\sigma}{d\overline{\omega}}(\omega)d\omega \tag{15}$$

is proportional to σ_d, the total cross section, and can be calculated from a two-dimensional integration of the differential cross section given on Fig. 4.

So, knowing that $\mathscr{D} \propto \sigma_d$ from relation (15) using figures such as Fig. 4 recorded for the different working energies, and $\overline{S}_d$ from Eq. (14) assuming $\theta=0$, we calculate the transmission ratio $k(E)/k(150)$ of the ion flux [relation (13)], which is normalized to 1 for $E_{c.m.} = 150$ eV (see Table II).

3. Absolute determination of the total diabatic cross section

The values of the diabatic cross section σ_d cannot be found directly in the literature. This is because the proba-
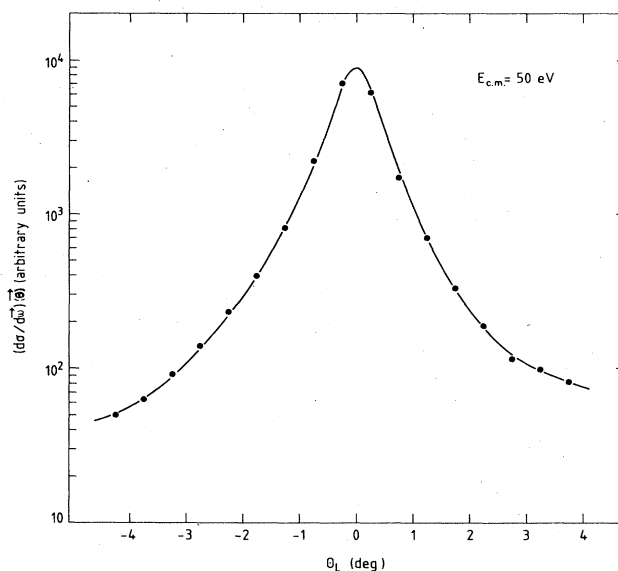

FIG. 4. Experimental differential ionization cross sections $(d\sigma/d\omega)_{\theta_L}$ of the $He^* + He$ system for the production of field-free He^+ ions, plotted as a function of the laboratory scattering angle θ_L. The zero scattering angle is determined from the symmetry of the positive and negative parts of the curve.

bility of reaching the continuum, starting from $He^*(2\ ^1S) + He(1\ ^1S)$ and $He^*(2\ ^3S) + He(1\ ^1S)$ (Fig. 1), via either of the diabatic curves involves two different kinds of curve crossings. (i) In the first (and also the less probable) a $2S \rightarrow 2P$ inelastic transition occurs over a wide zone which cannot be handled by Landau-Zener expressions. (ii) In the second a series of Landau-Zener crossings through the $n \geq 3$ levels between the first crossing and the continuum takes place. The system is assumed to immediately autoionize when the first ionization limit is reached. In the triplet case system, the first transition is obtained from the two-state close-coupling calculation of Evans et al.,[35] giving partial $2\ ^3S - 2\ ^3P$ cross sections at $E_{c.m.}$ values of 10, 50, 200, 400, and 500 eV. For our purpose, we have integrated them over the range of impact parameters leading to ionization (i.e., $R < 2.8a_0$). The

TABLE II. Lower limit of the diabatic cross-section values vs kinetic energy.

$E_{c.m.}$ (eV)	25	30	35	50	60	75	100	150
Transmission ratio $\dfrac{k(E)}{k(150)}$	2.5	2.03	1.83	1.39	1.34	1.27	1.16	1
$\dfrac{k(E)}{k(150)}\dfrac{S_d}{I^*} \propto \sigma_d$	7.3	11.2	14.1	26.1	40.8	66.8	147.9	303.7
σ_d (cm^2)	9×10^{-20}	1.4×10^{-19}	1.7×10^{-19}	$3.2 \times 10^{-19\,a}$	5.0×10^{-19}	8.2×10^{-19}	1.8×10^{-18}	3.7×10^{-18}

[a]Normalized value of σ_d at $E_{c.m.} = 50$ eV calculated from Ref. 35 (see Sec. III A 3).

subsequent transitions along the diabatic curve are given by Cohen[38] for the triplet system. There are no published values for the singlet one. The resulting values of σ_d are 8.8×10^{-21} cm^2 at $E_{c.m.} = 10$ eV, 3.2×10^{-19} cm^2 at 50 eV, and 6.3×10^{-18} cm^2 at $E_{c.m.} = 200$ eV (see Fig. 5). These values agree with other previously used values.[27,42]

So these values must be considered as the lower limits of our system since they correspond to the triplet diabatic channel. The presence of singlets in our experiment probably increases these cross sections, because the $2\,^1S-2\,^1P$ energy gap is smaller than the $2\,^3S-2\,^3P$ one. Hence, Fig. 5 represents the lower limit of the diabatic cross section σ_d for the field-free reaction (8), as a function of energy in the center-of-mass system. These results (solid circles) are normalized to the absolute value calculated from Ref. 35 at $E_{c.m.} = 50$ eV (Table II).

The curve drawn shows the good agreement between our results and the three aforementioned theoretical values (open circles) obtained. The error bars on the data include statistical uncertainties on the measurements and a 10% uncertainty in determining the relative transmission $k(E)/k(150)$.

B. Measurement of the contrast C

The contrast C is given by relation (11). It is obtained from the calculated values of D and A (see Fig. 6) for the

different working energies. The averaged background is obtained by removing the He($1\,^1S$) target, all the experimental parameters remaining unchanged. It was not possible to perform experiments for kinetic energies below $E_{c.m.} = 25$ eV because the statistical fluctuations of the field-free diabatic signal became too large: we can see in Fig. 6 that when $E_{c.m.} = 25$ eV the averaged value $\overline{S}_d$ only reaches 1.6 ions per channel. The behavior of C as a function of kinetic energy is shown on Fig. 7. All these experiments have been performed using either the YAG laser with a 20-mJ output energy, or the excimer laser set to give approximately the same pulse energy; the irradiated volume inside the collision cell, however, depends slightly on the energy distribution inside the assistance laser beam. So, we normalized all the contrasts to the values obtained using the excimer laser, the calibrating factor being 1.2. No attempt was made to take into account the effect due to the difference between the photon energies of the two laser beams ($\hbar\omega = 3.49$ eV for the YAG laser and $\hbar\omega = 3.53$ eV for the excimer laser). The major factor determining the uncertainty in C is the estimate of A, the integral of the assisted ion signal. The width of the window containing the laser-correlated ion contribution peak (Figs. 3 and 6) is obviously a function of the collisional kinetic energy through the He* atom crossing time t inside the interaction cell (see Sec. III). This time width roughly varies between six and three
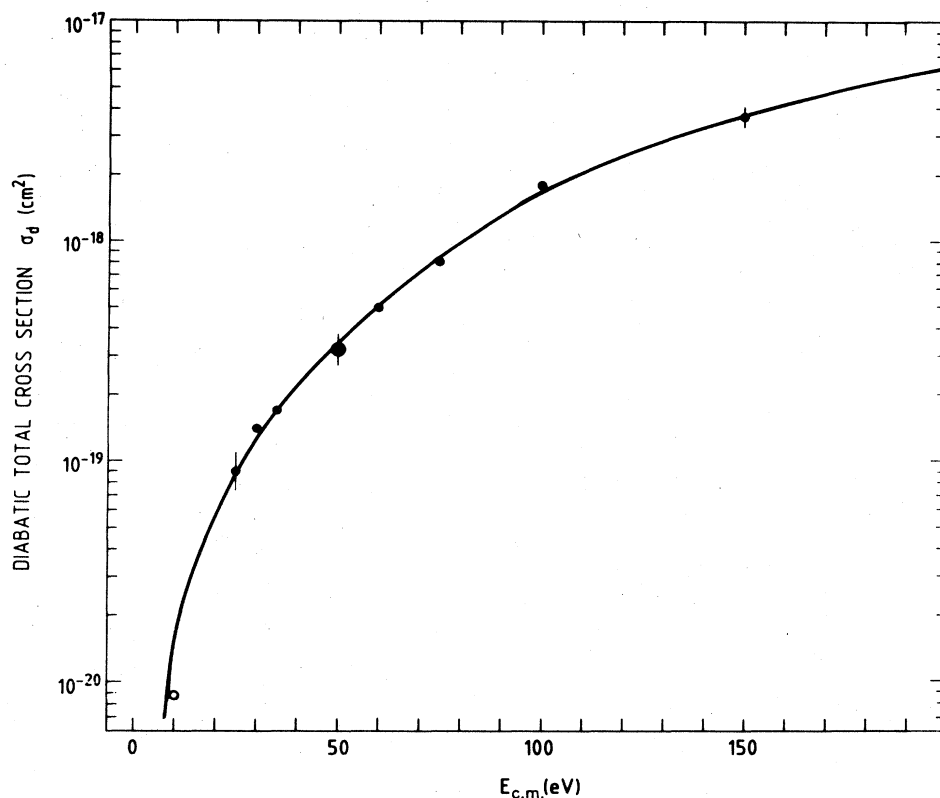

FIG. 5. Lower limit of the diabatic total cross section for the field-free reaction (8), vs the collision energy in the center-of-mass system. These results are normalized at $E_{c.m.} = 50$ eV to the calculated absolute value from Ref. 35. The open circles are obtained from the theoretical values of Evans *et al.* (Ref. 35).
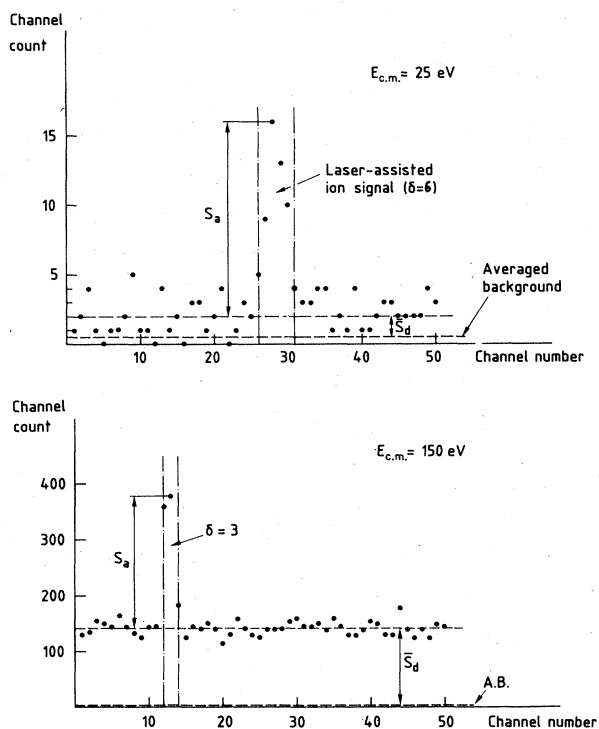
FIG. 6. Diabatic and assisted signal histograms obtained for $E_{\text{c.m.}} = 25$ and 150 eV. The assistance irradiation conditions are not the same and the data obtained for $E_{\text{c.m.}} = 150$ eV must be multiplied by 1.2 (YAG laser, see Sec. III B).

channels of the analyzer, whereas the colliding energy increases from 25 to 150 eV in the center-of-mass system as seen in Fig. 6. The error bars on the contrast C (Fig. 7) take a 5% statistical uncertainty in the data and a 10% uncertainty in the determination of the integral A into account.

With increasing energy, the contrast C decreases rapidly from 25 to 50 eV in the center-of-mass system then
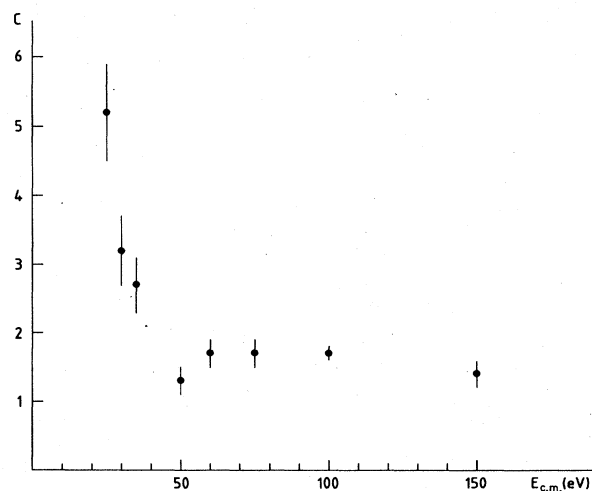

FIG. 7. Dependence of the contrast C on kinetic energy.

reaches a plateau until $E_{\text{c.m.}} = 150$ eV (Fig. 7). The colliding system represented by reaction (1) exhibits a completely different behavior as a function of kinetic energy: for energies less than about 50 eV in the center-of-mass system, the dominant ion-production mechanism is laser-assisted ionization; above $E_{\text{c.m.}} = 50$ eV the dominant ion-production process is a two-step reaction (see Sec. V B).

IV. RESULTS

A. Assisted ionization and the two-step-mechanism cross sections as a function of $E_{\text{c.m.}}$

The lower limit of σ_a can be deduced as a function of the colliding energy $E_{\text{c.m.}}$ from relation (12) using the values of σ_d given in Table II and the C values of Fig. 7. The behavior of σ_a as a function of $E_{\text{c.m.}}$ is shown on Fig. 8. It is clear that like C, σ_a exhibits two regions which overlap in the neighborhood of $E_{\text{c.m.}} = 50$ eV. The lower part of the curve ($E_{\text{c.m.}} < 50$ eV) decreases with increasing energy exhibiting a cross section which rapidly diminishes with the interaction time of the colliding partners (assisted ionization, Sec. IV B). On the contrary, above $E_{\text{c.m.}} = 50$ eV, the cross section increases with in-
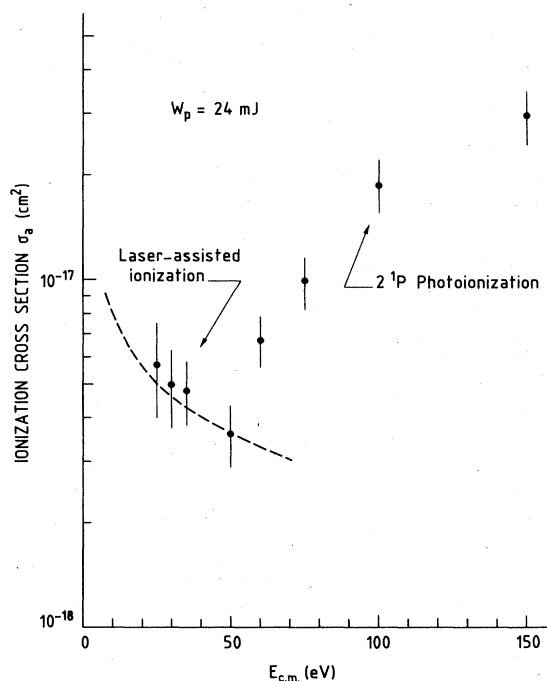

FIG. 8. Lower limit value of the assisted-ionization and two-step-mechanism ionization cross section vs the kinetic energy. The dots correspond to two regions: a region below $E_{\text{c.m.}} = 50$ eV where the dominant reaction is assisted ionization and another region above $E_{\text{c.m.}} = 50$ eV where the most important process is a collisional excitation followed by photoionization of the He** ($n \geq 2$). The dashed line represents the analytical expression $\sigma_a = (2.65 \times 10^{-17})/(E_{\text{c.m.}})^{1/2}$ and demonstrates the $1/v$ dependence of σ_a below $E_{\text{c.m.}} = 50$ eV.

creasing energy. In this case, ionization arises from a two-step reaction: collisional excitation of He* on the He target to reach an upper level followed by a photoionization of this level. It is clear that in this second process, the singlet system is widely prevalent (see Sec. V B).

B. Field intensity dependence of the assisted-ionization cross section

The assisted ion signal produced in reaction (1) is expected to increase linearly with light pulse energy, as relation (1) involves a single-photon absorption. This linear behavior has been made explicit in Ref. 28 with the expression giving the assisted ion signal produced in the interaction volume $\mathscr{V}$:

$$A = \sigma_\varphi \frac{I}{\hbar\omega} n_{\text{tm}} \tau \mathscr{V} , \tag{16}$$

where n_{tm} is the density of transient molecules able to be photoionized with a cross section σ_φ.[49] I is the averaged light power density and can be related to the pulse energy W_p by

$$W_p = I s \tau , \tag{17}$$

s is the cross-sectional area of the laser beam.

Combining (16) and (17) we can write
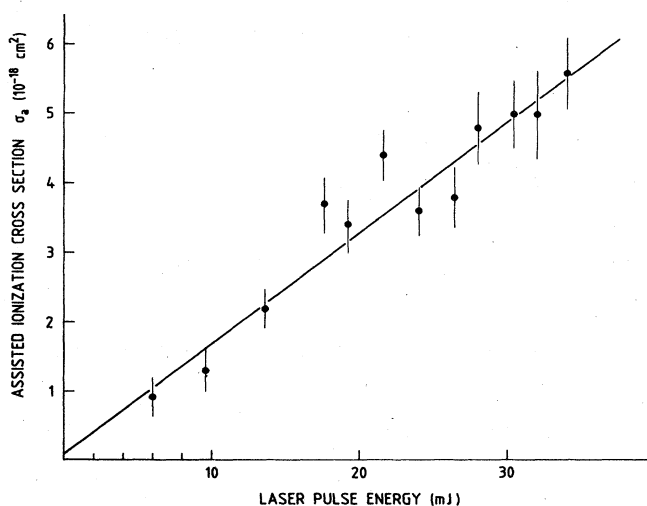
$$A \propto I$$

hence

$$A \propto W_p$$

and

FIG. 9. Assisted-ionization cross section vs laser pulse energy W_p for $E_{\text{c.m.}} = 50$ eV. The straight line is a linear regression calculation based on the experimental points. The resulting expression is $\sigma_a = 0.16\ W_p + 0.12$ with a correlation coefficient of 0.958. This curve has been normalized at $W_p = 24$ mJ to the $E_{\text{c.m.}} = 50$-eV value of Fig. 8, the experimental conditions being identical.

$$\sigma_a \propto W_p \tag{18}$$

for identical experimental conditions.

We verified the linear dependence of the assisted-ionization cross section on laser pulse energy W_p using the excimer laser over a dynamical range extending from 6 to 34 mJ. This test was performed under the same experimental conditions for a colliding energy of $E_{\text{c.m.}} = 50$ eV and takes 12 energy pulse values into consideration; it is presented in Fig. 9. This curve has been normalized at $W_p = 24$ mJ which corresponds to the same light assistance conditions as used in Fig. 8 (normalization to the excimer laser pulse, see Sec. III B). So the normalization point taken from Fig. 8 is $\sigma_a = 3.6 \times 10^{-18}$ cm^2 for $W_p = 24$ mJ. The straight line of Fig. 9 has been obtained by a linear-regression calculation based on the experimental points. The error bars represent the statistical error. The observed linearity is an important characteristic of the laser-assisted signal.[49]

V. DISCUSSION OF THE RESULTS

A. Validity of a one-photon absorption process

As outlined in Sec. I, the correctness of the laser-assisted picture depends on the strength and time scale of the collision and field perturbations. The proof that each measured ion is produced by single-photon absorption event is deduced from two experimental observations.

(i) the linearity of the assisted signal versus W_p (see Fig. 9).

(ii) the disappearance of the ion signal when employing photons with an energy below the photoionization threshold of the transient molecule, that is by irradiating the collision region with the fundamental frequency of the laser (i.e., $\hbar\omega = 1.16$ eV instead of 3.49 eV).

Therefore, the field-dressed curves for one-photon absorption plotted in Fig. 1 are well suited to describe process (1) in terms of a photoionization of the transient molecule. As already mentioned, the molecule is able to absorb radiation during a lifetime $t_m \sim 2R_0/v \sim 10^{-14}$ sec, whereas the laser period is 1.2×10^{-15} sec. Therefore, a photon description of the radiation field is correct. This holds because the bound-free process is allowed throughout the whole range of internuclear distances $R \leq R_0$. In our experimental conditions, this would be less correct for bound-bound transition, which would only be allowed over a much shorter period of time.

B. Dependence of σ_a on kinetic energy

It is not possible to obtain an exact expression for the laser-assisted cross section σ_a, since the radiative coupling terms between the initial potential curves and the continuum are not known as a function of R. However, an approximate and very simple expression can be obtained from the classical theory of Miller.[50] This will be used as a basis for discussing the magnitude of σ_a and its dependence on kinetic energy. The starting expression is[50]

$$\sigma_a = 2\pi \int_0^{R_0} b\, db \left[1 - \exp\left[-2 \int_b^{R_0} \frac{w(R)}{v_R(R)} dR \right] \right] , \tag{19}$$

where b is the impact parameter, v_R the radial component of the relative velocity, and $w(R)$ the photoionization probability per unit time. In our case, $w(R)=0$ for $R > R_0$ with $R_0=2.25$ and 1.95 Å, respectively, for the singlet and triplet system. The value of $w(R)$ is given by the Fermi golden rule, i.e., is proportional to the squared dipole matrix element between the initial and final molecular states. Since no analytical calculations of this element are available as a function of R, a simple approximation for (19) can be made by replacing $w(R)$ by its average value w inside the continuum. With this rough approximation, integration of (19) becomes possible. Assuming that $v_R(R) \sim v_\infty (1-b^2/R^2)^{+1/2}$ and that the exponential term in (19) is much smaller than unity, this gives

$$\sigma_a = \tfrac{4}{3}\pi R_0^3 \frac{w}{v_\infty} .$$

The photoionization cross section σ_φ for the transient molecule is $\sigma_\varphi = w/\mathscr{F}$, where $\mathscr{F}$ is the laser flux in $cm^{-2}\,sec^{-1}$; this leads to

$$\sigma_a = \tfrac{4}{3}\pi R_0^3 \frac{\sigma_\varphi \mathscr{F}}{v_\infty} , \qquad (20)$$

which shows that σ_a is approximately two-thirds of the geometrical cross section πR_0^2 of the transient molecules multiplied by the photoionization probability $\sigma_\varphi \mathscr{F} t_m$ during the time allowed for photon absorption $t_m = 2R_0/v_\infty$. Expression (20) is valid because $w(R)$ is assumed to be independent from R. With this assumption, σ_a is proportional to the lifetime t_m, i.e., to $1/v_\infty$.

This theoretical dependence is plotted in Fig. 8 and is seen to fit satisfactorily our experimental results for $E_{c.m.} \leq 50$ eV. For higher kinetic energy the observed dependence is completely different, that is increasing with $E_{c.m.}$ instead of decreasing. This is because as $E_{c.m.}$ increases, the assisted signal decreases and another process which is an increasing function of $E_{c.m.}$, becomes the dominant mechanism. This process is believed to be a two-step channel involving $2\,^1S \rightarrow 2\,^1P$ collisional excitation followed by photoionization of the $2\,^1P$. This hypothesis is based on a theoretical calculation[37] of the inelastic $2\,^1S - 2\,^1P$ cross section σ_{2P} showing two important characteristics: (i) σ_{2P} increases with $E_{c.m.}$ and (ii) high values of σ_{2P} are obtained ($\gtrsim 10^{-16}$ cm^2) because the transition occurs through angular coupling at the $2\,^1\Sigma_g - 2\,^1\Pi_g$ crossing (see Fig. 1). The triplet is not involved because our photon is below the $2\,^3P$ photoionization threshold. The $n \geq 3$ levels cannot contribute significantly to this ion production, because the collisional excitation of these levels from the $n=2$ level is highly improbable owing to large energy defects.

The rate equation for the $2\,^1P$ population is

$$\frac{dn(2P)}{dt} = \sigma_{2P} n^* nv - \sigma_\varphi' \mathscr{F} n(2P) - n(2P)/\tau' ,$$

where σ_φ' and τ' are, respectively, the photoionization cross section and the lifetime of the $2\,^1P$ level. The first term is the production rate from the $2\,^1S$ level, the second term the photoionization loss, and the third term the loss due to radiative decay.

Ion production from the $2\,^1P$ level can be expressed as follows:

$$\frac{dn'^+}{dt} = \sigma_\varphi' \mathscr{F} n(2P) .$$

The very short lifetime of the $2\,^1P$ level ($\tau' = 5 \times 10^{-10}$ sec, Ref. 51) makes $n(2P)$ nearly stationary during the laser pulse. Hence

$$n(2P) \simeq \sigma_{2P} n^* nv\tau' .$$

Ion production via this two-step channel can therefore be written

$$\frac{dn'^+}{dt} \simeq \sigma_{2P} \mathscr{F} \sigma_\varphi' \tau' n^* nv .$$

The theoretical dependence on $E_{c.m.}$ of this two-step ion production (nearly proportional to $E_{c.m.}^{1/2}$) from Ref. 37 does not agree with the experimental one (nearly proportional to $E_{c.m.}^2$). A possible explanation might be the contribution of the $2\,^1\Sigma_g$ state, which correlates asymptotically with the $He^*(2\,^1P)+He(1\,^1S)$ state, and which has not been taken into account in the two-state calculations of Ref. 37 at the $2\,^1\Sigma_g - 2\,^1\Pi_g$ crossing. However, more quantitative arguments are needed to more rigorously explain the observed discrepancy; such a treatment is beyond the scope of the present paper.

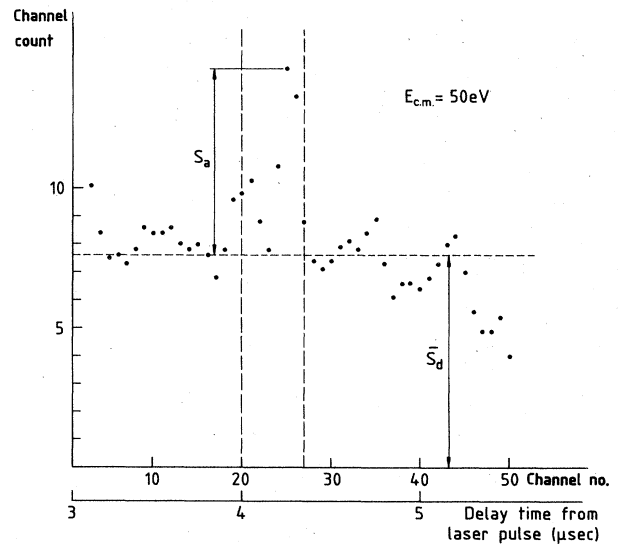The two-step channel does not contribute at $E_{c.m.} \leq 50$ eV, where the main contribution comes from the assisted

FIG. 10. Diabatic and assisted signal histograms for $E_{c.m.} = 50$ eV using a pure $2\,^3S$ metastable beam obtained by charge transfer of the He^+ primary beam on Na (see Sec. II). In spite of the very low statistical precision due to the fact that the He^* beam intensity obtained in this way is about 3 times lower (Ref. 46), it is clear that the assisted signal persists inside the vertical dash-dotted lines (laser-assisted signal window). This proves that for $E_{c.m.} = 50$ eV a two-step process (see Sec. V B) via the $2\,^1P$ state is not the principal mechanism for ion production in the He^* ($2\,^1S$, $2\,^3S$) beam case.

channel (1). This has been proved in a complementary experiment performed at $E_{c.m.} = 50$ eV with a pure $2\,^3S$ beam instead of the $2\,^1S + 2\,^3S$ mixed beam.[27] This pure beam was obtained by charge transfer of the He$^+$ primary beam on Na instead of Cs (Ref. 45) (reactions 5 and 6). Since the contrast remains almost unchanged with the pure $2\,^3S$ beam (see Fig. 10), and since the $2\,^3P$ cannot be photoionized by the 3.5 eV photon, it can therefore be concluded that the above described two-step process is not the main mechanism for ion production at this kinetic energy.

C. Competing processes

Depending on kinetic energy, laser intensity, etc., processes other than process (1) can produce ions. This is clearly apparent in Fig. 8 for $E_{c.m.} > 50$ eV. Conversely, for $E_{c.m.} \leq 50$ eV, process (1) is the only process which can explain the measured dependence of σ_a on $E_{c.m.}$ and on I. This has been verified by considering the following competing reactions.

(i) Two-photon ionization of He*($2\,^1S, 2\,^3S$): this process does not lead to the observed dependence of σ_a on I and $E_{c.m.}$. In addition, the presence of the He($1\,^1S$) perturber is not required; in our case, when the helium target is removed, there is no ion signal.

(ii) Photoexcitation of He*($2\,^1S, 2\,^3S$) followed by collisional ionization: the laser frequency is such that there is no resonant excitation from the He metastables. The smallest energy defect is ≥ 0.06 eV and occurs between the $2\,^1S + \hbar\omega$ and $5\,^1P$ atomic levels. The corresponding transition probability for this off-resonance excitation[52] is $\sim 2 \times 10^{-5}$. The resulting ionization cross section is thus less than 10^{-20} cm^2. Conversely, collision-induced photoexcitation may be possible: this laser-assisted collision would involve a bound-bound transition on a level which would ionize during the collision through crossings between the field-dressed curves and the $n \geq 3$ levels. This process has been shown[27] to give a negligible contribution. An upper limit of 6×10^{-21} cm^2 was determined using laser-assisted Landau-Zener cross sections.[49] This value is overestimated since the time available for photon absorption at each crossing is, under our conditions, of the order of or less than a laser period.

(iii) Collisional excitation of He*($2\,^1S, 2\,^3S$) followed by photoionization: field-free He* + He inelastic collisions may produce higher excited states which can be photoionized during the laser pulse. The order of magnitude of the population cross section for the $n \geq 3$ levels can be estimated from a Landau-Zener treatment using the radial coupling elements calculated by Cohen.[38] The result is that the total cross section for excitation of $n \geq 3$ levels is smaller than 10^{-19} cm^2 for $E_{c.m.} \leq 50$ eV and hence do not mainly contribute to the ion production. This has also been checked experimentally at $E_{c.m.} = 35$ eV from the time-of-flight (TOF) analysis of the ions, as follows: the time arrival of ions having exactly the same kinetic energy as the parent He* beam is determined in a separable experiment. A two-photon ionization process, via the $3\,^1P$ level, is performed without the He target, by using the second harmonic of the YAG laser ($\hbar\omega = 2.33$ eV).

Taking as origin on the multichannel analyzer (TOF scale) the arrival of these photoions, we can measure a delay and hence an energy defect for collisional processes. The sensitivity of this method, including time sampling and signal profiles is about 1 eV. The energy defects of the assisted signal coming from He($2\,^1S$) and He($2\,^3S$) metastable atoms are expected to be, respectively, 0.48 and 1.28 eV (see Fig. 1) while the energy defect of the ions coming from the two-step mechanism with $n \geq 3$ is at least 2.5 eV. The ion signal we observe corresponds to an averaged energy defect of 1.0 eV, which is coherent with the announced assisted process.

Following this two-step channel the most probable contributing process would be the $2\,^1S - 2\,^1P$ excitation (energy defect equal to 0.6 eV) but we have demonstrated in Sec. V B that the $2\,^1P$ photoionization contributes only for $E_{c.m.} > 50$ eV. In this two-step reaction, ion production has to increase with kinetic energy,[35-38] while we observe the opposite effect for energies below $E_{c.m.} = 50$ eV (Fig. 8).

D. Magnitude of the assisted cross section

The simple expression (20) for σ_a can be calculated using the photoionization cross-section value for the atomic metastables, i.e, $\sim 10^{-17}$ cm^2.[53] Comparison with the measured value of σ_a indicates the degree to which the atomic dipole is modified during the collision. Taking $E_{c.m.} = 50$ eV, $R_0 \sim 2$ Å, and $\mathscr{F} \sim 10^{25}$ cm^{-2} sec^{-1} ($W_p \sim 24$ mJ), one finds $\sigma_a \sim 10^{-21}$ cm^2. This is approximately 3 orders of magnitude smaller than what is measured. It can thus be concluded that during the collision, the $2S$ orbital of the optical electron is strongly modified, leading to a dipole transition moment ~ 30 times the unperturbed value. This is in qualitative agreement with the results of Guberman and Goddard[36] which indicate the $C\,^1\Sigma_g^+$ orbital to be highly distorted when $R \sim 2$ Å. At this sort of distance, exchange interaction plays a dominant role, and the collision system has a molecular structure very different from the atomic one. Other effects can also contribute to this strong dipole enhancement, for instance nonadiabatic effects induced by the high velocity of the collision system, or configuration effects in the He$^+$ + He + e$^-$ continuum. However, it seems difficult to check them quantitatively because of the insufficient accuracy of our experimental results.

VI. CONCLUSION

A laser-assisted ionization process has been studied by using a very low-density beam of helium metastables impinging on a He target under single-collision conditions in the presence of a nonresonant laser field. The simplicity of the system, the ability to monitor the kinetic energy of the collision, and time-of-flight detection of the ions have enabled us (i) to single out the assisted process from a field-free diabatic channel and a two-step process involving collisional excitation followed by photoionization (ii) to investigate, as a function of kinetic energy, both the field-free diabatic and the field-assisted cross sections, and

(iii) to deduce from a known value of the field-free diabatic cross section a lower limit for the assisted cross section, i.e., $\sigma_a \sim 4 \times 10^{-18}$ cm^2 for $E_{c.m.} = 50$ eV and $I \sim 5 \times 10^6$ Wcm^{-2}. The experiment shows that σ_a is a linear function of laser power density, and varies closely with the reciprocal of the relative velocity of the collision system. These two observations could lead to be a powerful way of checking laser assistance. Finally, the observed magnitude of σ_a corresponds to a dipole moment of the optical bound-free transition which is strongly enhanced during the collision.

[1]L. I. Gudzenko and S. I. Yakovlenko, Zh. Eksp. Teor. Fiz. 62, 1686 (1972) [Sov. Phys.—JETP 35, 877 (1972)].

[2]N. M. Kroll and K. M. Watson, Phys. Rev. A 13, 1018 (1976).

[3]M. H. Mittleman, Phys. Rev. A 14, 586 (1976).

[4]D. A. Copeland and C. L. Tang, J. Chem. Phys. 65, 3161 (1976); 66, 5126 (1977).

[5]S. Geltman, J. Phys. B 9, L569 (1976); 10, 3057 (1977).

[6]A. M. F. Lau and C. K. Rhodes, Phys. Rev. A 15, 1570 (1977).

[7]M. H. Nayfey and M. G. Payne, Phys. Rev. A 17, 1695 (1978).

[8]M. G. Payne, V. E. Anderson, and J. E. Turner, Phys. Rev. A 20, 1032 (1979).

[9]J. C. Bellum and T. F. George, J. Chem. Phys. 68, 134 (1978); 70, 5059 (1979).

[10]J. C. Bellum, K. S. Lam, and T. F. George, J. Chem. Phys. 69, 1781 (1978).

[11]P. L. De Vries and T. F. George, Phys. Rev. A 26, 1419 (1982).

[12]J. S. Dahler, R. E. Turner, and S. E. Nielsen, J. Phys. Chem. 86, 1065 (1982).

[13]H. P. Saha, J. S. Dahler, and S. E. Nielsen, Phys. Rev. A 28, 1487 (1983); H. P. Saha and J. S. Dahler, ibid. 28, 2859 (1983).

[14]K. S. Lam and T. F. George, Phys. Rev. A 32, 1650 (1985).

[15]S. E. Harris and D. B. Lidow, Phys. Rev. Lett. 33, 674 (1974).

[16]W. R. Green, J. Lukasik, J. R. Willison, M. D. Wright, J. F. Young, and S. E. Harris, Phys. Rev. Lett. 42, 970 (1979).

[17]J. C. White, Opt. Lett. 6, 242 (1981), and references therein.

[18]Ph. Cahuzac and P. E. Toschek, Phys. Rev. Lett. 40, 1087 (1978).

[19]C. Bréchignac, Ph. Cahuzac, and P. E. Toschek, Phys. Rev. A 21, 1969 (1980).

[20]A. Débarre, J. Phys. B 16, 431 (1983), with references therein.

[21]J. H. Goble, W. E. Hollingsworth, and J. S. Winn, Phys. Rev. Lett. 47, 1888 (1981).

[22]A. V. Hellfeld, J. Caddick, and J. Weiner, Phys. Rev. Lett. 40, 1369 (1978).

[23]P. Polak-Dingels, J. F. Delpech, and J. Weiner, Phys. Rev. Lett. 44, 1663 (1980).

[24]J. Weiner, Comments At. Mol. Phys. 16, 89 (1985), and references therein.

[25]F. Roussel, B. Carré, P. Breger, and G. Spiess, J. Phys. B 14, L313 (1981).

[26]B. Carré, F. Roussel, P. Breger, and G. Spiess, J. Phys. B 14, 4271 (1981).

[27]P. Pradel, P. Monchicourt, D. Dubreuil, J. Heuzé J. J. Laucagne, and G. Spiess, Phys. Rev. Lett. 54, 2600 (1985).

[28]P. Monchicourt, P. Pradel, F. Roussel, and J. J. Laucagne, Phys. Rev. A 33, 3515 (1986).

[29]A. Gallagher and T. Holstein, Phys. Rev. A 16, 2413 (1977).

[30]J. Szudy and W. E. Baylis, J. Quant. Spectrosc. Radiat. Transfer 15, 641 (1975); 17, 681 (1977).

[31]J. Huennekens and A. Gallagher, Phys. Rev. A 27, 771 (1983).

[32]J. Keller and J. Weiner, Phys. Rev. A 30, 213 (1984).

[33]C. E. Burkhardt, W. P. Garver, and J. J. Leventhal, Phys. Rev. A 31, 505 (1985).

[34]F. Roussel, P. Breger, and G. Spiess, J. Phys. B 18, 3769 (1985).

[35]S. A. Evans, J. S. Cohen, and N. L. Lane, Phys. Rev. A 4, 2235 (1971). The cross-section values of Table I should be read in units of $10^{16}a_0^2$ instead of cm^2.

[36]S. L. Guberman and W. A. Goddard III, Chem. Phys. Lett. 14, 460 (1972); Phys. Rev. A 12, 1203 (1975).

[37]E. J. Shipsey, J. C. Browne, and R. E. Olson, Phys. Rev. A 11, 1334 (1975).

[38]J. S. Cohen, Phys. Rev. A 13, 86 (1976).

[39]R. P. Saxon, K. T. Gillen, and B. Liu, Phys. Rev. A 15, 543 (1977).

[40]R. Morgenstern, D. C. Lorents, J. R. Peterson, and R. E. Olson, Phys. Rev. A 8, 2372 (1973).

[41]R. E. Olson, R. Morgenstern, D. C. Lorents, J. C. Browne, and L. Lenamon, Phys. Rev. A 8, 2387 (1973).

[42]K. T. Gillen, D. C. Lorents, R. E. Olson, and J. R. Peterson, J. Phys. B 7, L327 (1974).

[43]K. T. Gillen, J. R. Peterson, and R. E. Olson, Phys. Rev. A 15, 527 (1977).

[44]A general definition of field-free Penning ionization is given by A. Niehaus, in Invited Papers of the Twelfth International Conference on the Physics of Electronic and Atomic Collisions, Gatlinburg, 1981, edited by S. Datz (North-Holland, Amsterdam, 1982), p. 237. Experiments concerning laser-induced Penning ionization processes can be found in Refs. 21—24.

[45]C. Reynaud, J. Pommier, Vu Ngoc Tuan, and M. Barat, Phys. Rev. Lett. 43, 579 (1979).

[46]V. Sidis, C. Kubach, and J. Pommier, Phys. Rev. A 23, 119 (1981).

[47]P. Pradel and J. J. Laucagne, J. Phys. (Paris) 44, 1263 (1983).

[48]H. Scheidt, G. Spiess, A. Valance, and P. Pradel, J. Phys. B 11, 2665 (1978).

[49]S. I. Yakovlenko, Kvant. Elektron. (Moscow) 5, 259 (1978) [Sov. J. Quantum Electron. 8, 151 (1978)].

[50]W. H. Miller, J. Chem. Phys. 52, 3563 (1970).

[51]W. L. Wiese, M. W. Smith, and B. M. Glennon, Atomic Transition Probabilities, Natl. Stand. Ref. Data Ser., Natl. Bur. Stand. (U.S.) Circ. No. 4 (U.S. GPO, Washington, D.C., 1966), Vol. 1.

[52]C. Cohen Tannoudji, B. Diu, and F. Laloë, Mécanique Quantique (Hermann, Paris, 1973), Vol. II.

[53]R. F. Stebbings, F. B. Dunning, F. K. Tittel, and R. D. Rundel, Phys. Rev. Lett. 30, 815 (1973).